IEEE Transactions on Industrial Electronics, pp. 1–1, 2019

Multi-Variable High-Frequency Input-Admittance of Grid-Connected Converters: Modeling, Validation and Implications on Stability

F. D. Freijedo, M. Ferrer-Duran, and D. Dujic

POWER ELECTRONICS LABORATORY
ÉCOLE POLYTECHNIQUE FÉDÉRALE DE LAUSANNE

This article has been accepted for publication in a future issue of this journal, but has not been fully edited. Content may change prior to final publication. Citation information: DOI 10.1109/TIE.2019.2892701, IEEE Transactions on Industrial Electronics

Multi-Variable High-Frequency Input-Admittance of Grid-Connected Converters: Modeling, Validation and Implications on Stability

Francisco D. Freijedo, *Senior Member, IEEE*, Marc Ferrer and Drazen Dujic, *Senior Member, IEEE*

***Abstract*—Modern grids are facing a massive integration of power electronics devices, usually associated to instability issues. In order to assess the likelihood and severity of harmonic instability in the high frequency region, this work develops a multi-variable input-admittance model that accurately reflects the following aspects: i) the discrete controller frequencies are defined inside a spectrum region limited by the Nyquist frequency; ii) the physical system aliases are transformed into lower frequency component inside the discrete controller. The proposed model shows that dynamic interactions are not theoretically band-limited; however, the control action tends to be strongly limited in a low frequency range, due to the natural low-pass filter behavior of acquisition and modulation blocks. This is reflected in a reduced resistive part (either positive or negative) of the input-admittance in the high frequency range. More specifically, considering the input-admittance passivity criterion, the excursions into the non-passive area are very smooth at high frequencies, where the input-admittance is well described by simply its inductive filter. Comprehensive experiments are conducted on a lab scale prototype, which includes measurements beyond the Nyquist frequency and alias identification. The experimental results well match the theoretical model.**

Index Terms - Ac/dc power conversion, Admittance Measurement, Pulse width modulated power converters, Stability Criteria.

I. Introduction

Modern grids are facing a massive integration of power electronics equipment aiming for a higher system level design flexibility, sustainability and improved performance and efficiency. However, large integration of power converters based on high-bandwidth closed-loop controllers poses new challenges to the stability and power quality. In this sense, several incidents have been reported in high-speed electric train and renewable energy applications [1]–[3]. Due to the paramount importance of renewable energy integration and electric transportation, research on dynamic interactions among active devices in complex grids is on the rise [2]–[8]. Among others, impedance modeling approaches and stability criteria are suitable frameworks to address controllers design and dynamics assessment of power systems dominated by power electronics [fundamental theory and application of the single-input single-output (SISO) impedance stability criteria, including an example based on grid-connected converter, are reviewed in the appendix] [1]–[15]. A key feature of impedance/admittance methodologies is the fact that they are able to deal with the presence of high uncertainty in the physical model: e.g., the input-admittance passivity criterion is a stringent requirement that aims for robustness of the grid-connected equipment [1], [5], [8], [16]. Input-admittance passivity compliance is a requirement already reflected in the EN50388 Ed. 2 standard issued for railway applications [5], [8], [16], [17]. The SISO input-admittance passivity criterion for grid-connected converters is applied as follows [3]:

- firstly, the environment model is assumed unknown, but passive; i.e., for $Z_g(\omega)$ being the grid impedance, $\mathrm{Re}\{Z_g(\omega)\} \geq 0$, or equivalently $|\angle Z_g(\omega)| \leq 90\,\mathrm{deg}$.
- subsequently, stability is assured if the input-admittance, defined as $Y(\omega)$, is also passive; i.e., $\mathrm{Re}\{Y(\omega)\} \geq 0$ (i.e., $|\angle Y(\omega)| \leq 90\,\mathrm{deg}$).

Even though in principle the passivity criteria applies to all the region of the spectrum, the EN50388 Ed. 2 standard defines a range of the fifth harmonic (e.g., $250\,\mathrm{Hz}$ for $50\,\mathrm{Hz}$ grids) to the Nyquist frequency (defined by the controller sampling frequency) [3], [8], [16]–[18]. This finite frequency approach has been theoretically proved as suitable to deal with stability problems involving realistic active controllers, which in practice are not ideal and are band-limited [19], [20]. Therefore, an explicit band-limitation for the passivity compliance should be included in system specifications and controller design problems [8], [18]–[20]. Recent studies have reported some contradictory observations that make difficult to clearly set a region for passivity compliance of grid-connected converters (i.e., below or higher than the Nyquist frequency): on the one hand, the control action is more and more reduced in the high frequency range [5], [21], which suggests that passivity assessment can be studied to a range well below the Nyquist frequency; however, instability due to harmonic interactions at very high frequencies (even beyond the Nyquist one) are possible [8]. More specifically, an elaborated input-admittance model, which considers the PWM, sample and hold and aliasing terms, is developed in [8]; that work also provides time-domain waveforms that show undamped responses when the system plant has a resonance around the Nyquist frequency. With acknowledge to the main ideas presented in [8],

Manuscript received June 14, 2018; revised September 17, 2018 and November 28, 2018; accepted December 4, 2018.

This work was supported in part by the Swiss Federal Office of Energy under the Project "Medium-Voltage Direct-Current Energy Conversion Technologies and Systems (SI/501259)".

Francisco D. Freijedo (corresponding author) and Drazen Dujic are with the Power Electronics Laboratory, EPFL, CH1005, Lausanne, Switzerland. E-mails: francisco.freijedo@epfl.ch (Tel: +41 21 693 47 89 and Fax: +41 21 693 26 00) and drazen.dujic@epfl.ch.

Marc Ferrer was with the Escola Tecnica Superior d'Enginyeria Industrial de Barcelona, Universitat Politecnica de Catalunya, Catalunya, Spain (M.Sc Student). E-mail: marc.ferrer.duran@estudiant.upc.edu.

This article has been accepted for publication in a future issue of this journal, but has not been fully edited. Content may change prior to final publication. Citation information: DOI 10.1109/TIE.2019.2892701, IEEE Transactions on Industrial Electronics

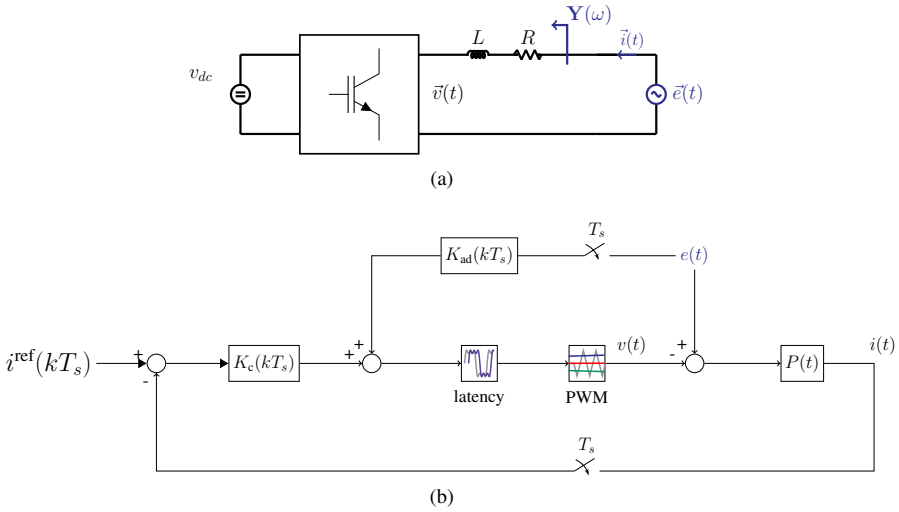

Fig. 1. System under study. a) Simplified VSC circuit. b) Discrete-time closed loop current controller.

this paper deepens on the concept of multi-frequency input-admittance model and provides comprehensive experimental results in the frequency-domain. The main theoretical goal is to accurately weight the factors that tend to limit the control action (i.e., low-pass filtering of the plant, A/D and PWM [21]) versus the active controller actions (i.e., proportional control and active damping), and support the modeling with a comprehensive frequency-domain experimental validation. With regard to previous state-of-the-art, main contributions of this work are:

1) For a given grid-connected converter, an input-admittance modeling methodology that accurately describes the behavior in the very high frequency range has been developed: its multi-variable structure permits to consider alias terms in order to extend the assessment region beyond the Nyquist frequency. The model is directly developed in the frequency domain; this strategy permits to describe discrete and continuous physical processes separately and, eventually, integrate all of them in the whole model. One remarkable approach is the modelling of the A/D acquisition to reflect the aliasing effect (lumping of multiple alias in a single frequency component) by the Z-domain describing function approach [22], [23]; by this technique, the discrete-controller only sees components in the region of the spectrum delimited by the Nyquist frequency.
2) The accuracy of the input-admittance model in the frequency domain has been verified in the laboratory by a comprehensive set of experiments. A high performance grid simulator and a grid-connected converter working with a low sampling frequency operation have been employed to obtain the figures of merit. Overall, the experimental results confirm the accuracy of the theoretical approach and permits to obtain important conclusions about the role of A/D and PWM blocks, and the severity of alias interactions. Active damping action, which permits to move the non-passive regions to higher regions of the spectrum is also assessed. The proposed input-admittance modelling has been proved to be an accurate and reliable representation of the converter dynamics at high frequency ranges, including components beyond the Nyquist frequency.

The rest of the paper is organized as follows. Section II provides a description of the problem. Section III presents the multi-variable input-admittance concept, which is designed to include high-frequency interactions. Section IV provides detailed derivations of the blocks involved in the discrete process. Section V shows and analyzes the experimental results that verify the theoretical approach. Finally, the contributions to the state-of-the-art are summarized.

II. System and Problem Descriptions

Fig. 1(a) shows a simplified single-line representation of a grid-connected converter, with $i(t)$, $v(t)$ and $e(t)$ being the current, the converter output and the grid voltage, respectively. The converter interfaces the grid through a filter, which is formed by an inductance L (including its series resistor R). Assuming a SISO system and linear relation between electric variables, the input-admittance is defined in the frequency domain by $Y(\omega) = i(\omega)/e(\omega)$.

The converter is an active device able to shape $Y(\omega)$ at the range of frequencies for which the closed-loop actuation is not negligible. In principle, considering reference tracking and disturbance rejection, this range is upper bounded around $0.1\omega_s$, with ω_s being the controller sampling frequency. However, the range of actuation is extended well beyond when considering side-effects that may create a positive feedback of high frequency components, including potential interactions of components beyond the Nyquist frequency $0.5\omega_s$ [8].

The input-admittance shape in the frequency domain can be obtained from the relation between the loop perturbation $e(\omega)$ and the controlled variable $i(\omega)$ [9]. Fig. 1(b) shows a discrete-time closed-loop current controller, which includes:

1) The A/D acquisition of electric variables.
2) A main controller $K_{\text{c}}(kT_s)$ and an active damping action $K_{\text{ad}}(kT_s)$.

This article has been accepted for publication in a future issue of this journal, but has not been fully edited. Content may change prior to final publication. Citation information: DOI 10.1109/TIE.2019.2892701, IEEE Transactions on Industrial Electronics

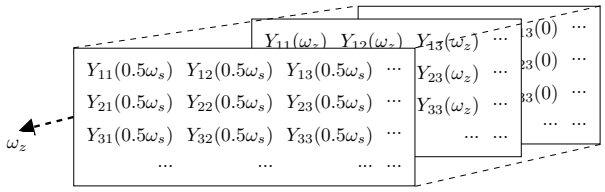

Fig. 2. Multi-variable $\mathbf{Y}(\omega_z)$ definition in the frequency domain for a group of alias up to $N = 3$: the subscript "1" correspond to input/output main components; the subscripts not equal to "1" correspond to the successive input/output alias components.

3) An average delay between the A/D acquisition and update of PWM registers.
4) The PWM block which calculates the firing pulses from its reference.

All of these components are included in the multi-variable frequency domain matrix that represents the input-admittance. Relevant assumptions, which are in good agreement to the application of the EN50388 Ed. 2 standard [16], are:

- The current reference $i_{\text{ref}}(\omega)$ is considered zero in the range of frequency of interest [no load operation]; this is reasonable in the sense that typical bandwidths of outer-controllers are much lower than the fifth harmonic $250\,\text{Hz}$ [8], [18].
- For three-phase system, a per-phase decoupled model is considered. This assumption is supported by the fact that the controllers aiming for a zero steady-state error (e.g., integrators in the dq-frame) are also operating in the very low frequency region of the spectrum (i.e., at 50 Hz) [5].
- Non-linearities such as side-band harmonics generation as a function of the fundamental ($50\,\text{Hz}$) output voltage component (i.e., operation point) are not considered, since the multi-variable input admittance is linear. In that sense, a differential modelling of the PWM block is employed, which allow to keep the problem as a linear one [24].

Some of these assumption imply to over-simplify the model for the very low frequency ranges (e.g., effects of outer loops are discarded) in order to develop an insightful high frequency model. For studies related to dynamics in the low frequency range, such as interactions of the phase locked loop with the current controllers, references [4], [10], [14] may be suggested.

III. Multi-Variable Input-Admittance

Fig. 2 depicts the proposed multi-variable input-admittance concept. The input-admittance $\mathbf{Y}(\omega_z)$ is defined in for frequencies in the range $\omega_z \in [0, 0.5\omega_s)$; i.e., the Nyquist-Shannon sampling theorem is considered to set the upper limit for the discrete process [25]. For the sake of clarity, a nomenclature similar to the one employed in harmonic studies is employed: the subscript "1" correspond to input/output fundamental components (i.e., the components that in the real physical domain have already a frequency below $\omega_s/2$); the subscripts not equal to "1" correspond to the successive input/output alias components. The ellipsis employed in Fig. 2, and in several equations next, represent the fact that, theoretically, there is no limit for the number of alias to consider. However, in practice, a frequency band-limitation has to be introduced for theoretical/numerical analyses and experimental verification [19], [20]. E.g., due to the limited text linewidth, the number of alias explicitly written in the theoretical analysis, hereby defined by N, is 3.

Fig. 3 shows the multi-variable loop employed to derive $\mathbf{Y}(\omega_z)$. The converter current is

$$\vec{i}(\omega_z) = \begin{bmatrix} i(\omega_z) & i(\omega_s - \omega_z) & i(\omega_s + \omega_z) & ... \end{bmatrix}^T \quad (1)$$

and the disturbance voltage is

$$\vec{e}(\omega_z) = \begin{bmatrix} e(\omega_z) & e(\omega_s - \omega_z) & e(\omega_s + \omega_z) & ... \end{bmatrix}^T. \quad (2)$$

Therefore, the relation between system variables and input-admittance is

$$\vec{i}(\omega_z) = \mathbf{Y}(\omega_z) \cdot \vec{e}(\omega_z). \quad (3)$$

The control action, i.e., the converter output is

$$\vec{v}(\omega_z) = \begin{bmatrix} v(\omega_z) & v(\omega_s - \omega_z) & v(\omega_s + \omega_z) & ... \end{bmatrix}^T. \quad (4)$$

The system plant relates the system variables as follows

$$\vec{i}(\omega_z) = \mathbf{P}(\omega_z) \cdot [\vec{e}(\omega_z) - \vec{v}(\omega_z)]. \quad (5)$$

The plant matrix is

$$\mathbf{P}(\omega_z) = \begin{bmatrix} \frac{1}{j\omega_z L + R} & 0 & 0 & 0 \\ 0 & \frac{1}{j(\omega_s - \omega_z)L + R} & 0 & 0 \\ 0 & 0 & \frac{1}{j(\omega_s + \omega_z)L + R} & 0 \\ 0 & 0 & 0 & \ddots \end{bmatrix}. \quad (6)$$

From Fig. 3, the control action is a function of controller implementation

$$\begin{aligned} \vec{v}(\omega_z) = {} & \vec{H}_{\text{sw}}(\omega_z) e^{-jT_d\omega_z} K_{\text{c}}(\omega_z) \vec{N}(\omega_z) \vec{i}(\omega_z) \\ & - \vec{H}_{\text{sw}}(\omega_z) e^{-jT_d\omega_z} K_{\text{ad}}(\omega_z) \vec{N}(\omega_z) \vec{e}(\omega_z) \end{aligned} \quad (7)$$

with $\vec{H}_{\text{sw}}(\omega_z)$, $\vec{N}(\omega_z)$, T_d, $K_{\text{c}}(\omega_z)$ and $K_{\text{ad}}(\omega_z)$ modelling the PWM block, the A/D acquisition, the latency delay, the main controller and the active damping controller, respectively. From (3), (5) and (7) and basic matrix algebra, the system admittance matrix is obtained as

$$\begin{aligned} \mathbf{Y}(\omega_z) = {} & [\mathbf{I} + \mathbf{P}\vec{H}_{\text{sw}}(\omega_z) K_{\text{c}}^{'}(\omega_z) \vec{N}(\omega_z)]^{-1} \\ & \cdot [\mathbf{P} + \mathbf{P}\vec{H}_{\text{sw}}(\omega_z) K_{\text{ad}}^{'}(\omega_z) \vec{N}(\omega_z)]. \end{aligned} \quad (8)$$

with $K_{\text{c}}^{'}(\omega_z)$ and $K_{\text{ad}}^{'}(\omega_z)$ representing the control actions with their associated delay. The next section provides a detailed modeling of each process giving rise to a characterization of all the components of (8). It should be noticed that the result of (8) should be a $N \times N$ matrix.

IV. Modelling the Discrete-Domain Processes

From the definition in (8), Fig. 4 depicts the hybrid modelling strategy employed to calculate $\mathbf{Y}(\omega)$. Clearly, the main challenges of modelling point to the discrete process, which is divided in three parts: the A/D acquisition, modelled by the Z-transform describing function technique [22], [23], the discrete controller operations and the PWM output generation. These

This article has been accepted for publication in a future issue of this journal, but has not been fully edited. Content may change prior to final publication. Citation information: DOI 10.1109/TIE.2019.2892701, IEEE Transactions on Industrial Electronics

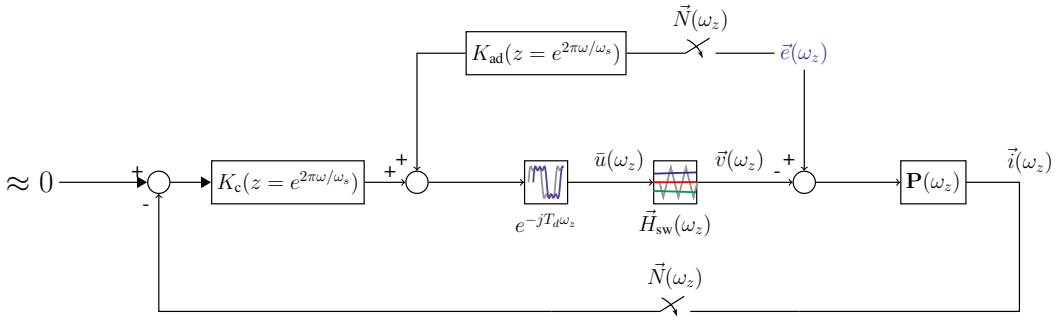

Fig. 3. Representation of the current controller loop employed to derive $\mathbf{Y}(\omega_z)$.

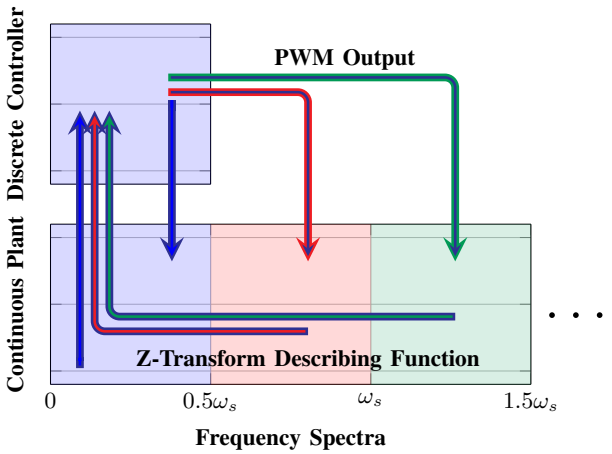

Fig. 4. Conceptual schema of the hybrid modelling strategy for $\mathbf{Y}(\omega)$ calculation (the background colors represent different alias regions).

blocks, which relate two inputs [$\vec{i}(\omega_z)$ and $\vec{e}(\omega_z)$] with the control action [$\vec{i}(\omega_z)$], are described in the next subsections.

A. Z-Transform Describing Function for A/D Acquisition

In order to obtain a frequency response that relates a continuous domain input signal of any arbitrary frequency ω to its discrete first alias a describing function approach is followed [22], [23]; i.e., for a given input $\vec{i}(\omega_z)$ [or $\vec{e}(\omega_z)$, cf. Fig. 3], the idea is to find the average value $\bar{u}(\omega_z)$ that holds during the sampling period. Since $\bar{u}(\omega_z)$ is a function of the multiple input alias, the describing function is modeled as a multi-variable transfer function $\vec{N}(\omega_z, \omega_s)$, defined as

$$\bar{i}(\omega_z) = \vec{N}(\omega_z, \omega_s)\vec{i}(\omega_z, \omega_s). \tag{9}$$

$\vec{N}(\omega_z, \omega_s)$ is modelled as follows. Firstly, a time-domain signal of unit amplitude and frequency $\omega_z < 0.5\omega_s$ (this range is set according the Nyquist-Shannon sampling theorem) is

$$i_1(t) = \cos(\omega_z t) = \frac{e^{j\omega_z t} + e^{-j\omega_z t}}{2}. \tag{10}$$

The acquired signal, averaged over a sampling cycle ($T_s = 2\pi/\omega_s$) is

$$\begin{aligned}\bar{i}(\omega) &= \underbrace{\Big[\frac{1}{T_s}\sum_{n=-\infty}^{\infty} i_1(\omega_z + n\omega_s)\Big]}_{i_1^*(\omega_z)} \cdot \underbrace{\frac{1-e^{j2\pi\omega/\omega_s}}{j\omega}}_{G_{\text{s}}(\omega)} = \\ &= \frac{1}{T_s}\sum_{n=-\infty}^{\infty} i_1(\omega_z + n\omega_s)G_{\text{s}}(\omega_z + n\omega_s).\end{aligned} \tag{11}$$

with $i_1^*(\omega_z)$ defining the starred transform and $G_{\text{s}}(\omega)$ the zero-order hold (ZOH) transfer function filter associated to the sampling process [25]. On the other hand, the sought describing function $N_1(\omega_z, \omega_s)$ defines the relation between $i_1(\omega_z)$ and $\bar{i}(\omega_z)$ [22], [23].

$$\bar{i}(\omega_z) = N_1(\omega_z, \omega_s)i_1(\omega_z). \tag{12}$$

Equation (12) can be solved from the impulse response, where $i_1(t) = \delta(t)$ is now considered as an input in the time domain [25]. Evaluation in the Fourier domain of the impulse response is straightforward, since it is based on the substitution $i_1(\omega_z + n\omega_s) = 1 \ \forall \ n = 0, \pm1, \pm2, ...$ in (11).

$$\begin{aligned}N_1(\omega_z, \omega_s) =& \bar{i}(\omega_z)|_{i(\omega_z+n\omega_s)=1 \ \forall \ n=0,\pm1,\pm2,...} \\ &= \sum_{n=-\infty}^{\infty} G_{\text{s}}(\omega_z + n\omega_s).\end{aligned} \tag{13}$$

Expanding (13) up to $N = 4$, gives

$$\begin{aligned}N_1(\omega_z, \omega_s) =& G_{\text{s}}(\omega_z) + G_{\text{s}}(\omega_z - \omega_s) + G_{\text{s}}(\omega_z + \omega_s) \\ &+ G_{\text{s}}(\omega_z - 2\omega_s) + ...\end{aligned} \tag{14}$$

Now, an input in the first alias region is considered:

$$i_2(t) = \cos[(0.5\omega_s + \omega_z)t] = \frac{e^{j(0.5\omega_s+\omega_z)t} + e^{-j(0.5\omega_s+\omega_z)t}}{2}. \tag{15}$$

From (15), it is straightforward to identify that

$$\begin{aligned}i_2^*(\omega_z) =& \frac{1}{T_s}\sum_{n=-\infty}^{\infty} i(\omega_z + 0.5\omega_s + n\omega_s) = \\ &- \frac{1}{T_s}\sum_{n=-\infty}^{\infty} i(\omega_z + n\omega_s) = -i_1^*(\omega_z),\end{aligned} \tag{16}$$

This article has been accepted for publication in a future issue of this journal, but has not been fully edited. Content may change prior to final publication. Citation information: DOI 10.1109/TIE.2019.2892701, IEEE Transactions on Industrial Electronics

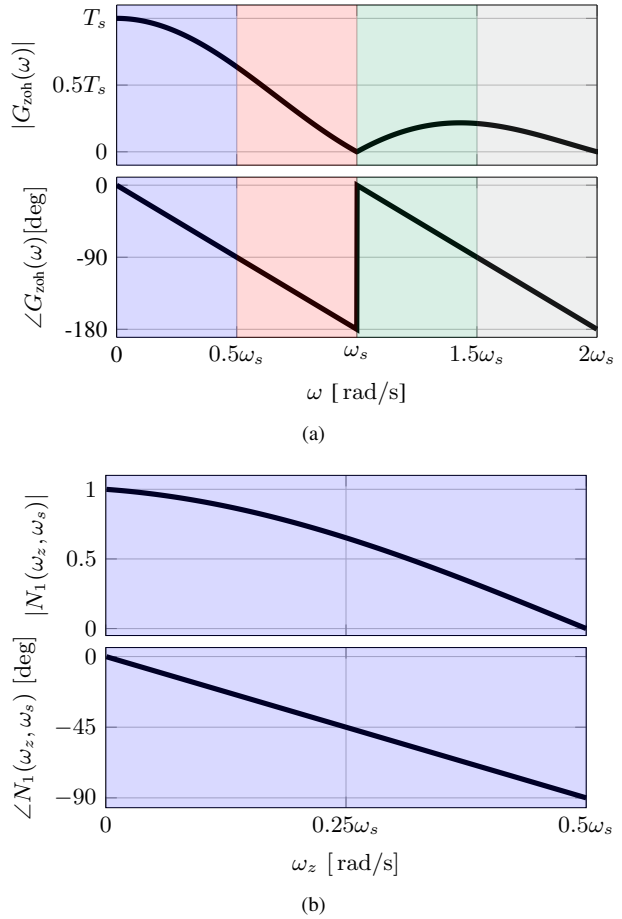

Fig. 5. Frequency responses of A/D acquisition filters. a) $G_{\text{zoh}}(\omega)$ with alias regions. b) Discrete describing function $N_1(\omega_z, \omega_s)$.

which immediately leads to

$$N_2(0.5\omega_s + \omega_z, \omega_s) = -N_1(\omega_z, \omega_s). \tag{17}$$

Finally, considering the whole input vector, the discrete signal after the ZOH can be defined as with

$$\vec{N}(\omega_z, \omega_s) = N_1(\omega_z, \omega_s)\begin{bmatrix}1 & -1 & 1 & -1 & ...\end{bmatrix}. \tag{18}$$

Fig. 5 shows the frequency responses of $G_{\text{zoh}}(\omega)$ and $N_1(\omega_z, \omega_s)$. It should be noticed that $N_1(\omega_z, \omega_s)$ is a low-pass filter (describing function), which well models the regular sampling filtering: its gain is ≈ 1 at the low frequencies and ≈ 0 zero near the Nyquist frequency $\omega_s/2$ [21]. It should be also recalled that the Z-Transform Describing Function technique that models the A/D acquisition groups the continuous domain components, of any arbitrary frequency, in a well delimited region of the spectrum bounded by Nyquist frequency $\omega_s/2$.

B. Calculation of $K_c^{'}(\omega_z)$ and $K_{ad}^{'}(\omega_z)$

Discrete-time controllers are implemented by difference equations, and therefore, accurately modeled by conventional Z-domain transfer functions [25]. The main controller and active damping action are defined in Fig. 1(b) as scalar discrete transfer functions $K_{\text{c}}(z)$ and $K_{\text{ad}}(z)$. In principle, $K_{\text{c}}(z)$ can be a Proportional-Integral (PI) or Proportional-Resonant (PR) controller. $K_{\text{ad}}(z)$ can be a derivative active damping of the form $K_{\text{ad}}(z) = k_{ad}\frac{1-z^{-1}}{T_s}$, with $T_s = 2\pi/\omega_s$ being the controller sampling rate [9]. The frequency domain equivalents are obtained by the variable substitution $z = e^{j2\pi\omega_z/\omega_s}$ [25].

Since there is a latency or delay between the acquisition of electric variables and the update of the PWM registers, a pure system delay T_d can be added at this stage. The resultant frequency domain expressions of the discrete-controller are

$$K_{\text{c}}^{'}(\omega_z) = e^{-j2\pi T_d\omega_z}K_{\text{c}}(z = e^{j2\pi\omega_z/\omega_s}) \tag{19}$$

and

$$K_{\text{ad}}^{'}(\omega_z) = e^{-j2\pi T_d\omega_z}K_{\text{ad}}(z = e^{j2\pi\omega_z/\omega_s}). \tag{20}$$

C. PWM Output and Generation of Alias

The PWM block generates the firing signals that construct the control action and therefore, interfaces back the discrete controller with the physical system by re-injecting the main but also alias components [18], [24], [26]. Fig. 6 shows time domain and its corresponding spectrum for a small signal differential PWM model. The magnitude of the PWM component and its switching alias can be approximated by [18], [24], [26]

$$H_{\text{sw}}(\omega) = \frac{1}{T_{\text{sw}}}\Big|\underbrace{\frac{1 - e^{j\omega T_{\text{sw}}}}{j\omega}}_{G_{\text{sw}}}\Big|. \tag{21}$$

It should be noticed that the switching cycle T_{sw} instead of T_s is employed. From a given reference $\bar{u}(\omega_z)$ (obtained by the discrete controller, and hence, defined in the range $[0, 0.5\omega_s]$) the PWM output is modelled by

$$\vec{u}(\omega_z) = \vec{H}_{\text{sw}}(\omega_z)\bar{u}(\omega_z) \tag{22}$$

with

$$\vec{H}_{\text{sw}}(\omega_z) = [H_{\text{sw}}(\omega_z) \;\; H_{\text{sw}}(\omega_s - \omega_z) \;\; H_{\text{sw}}(\omega_s + \omega_z) \;\; ...]^T. \tag{23}$$

Fig. 7 shows the frequency domain representation of the multi-variable PWM model. Single and double update strategies are both depicted (the background colors represent different alias regions). Similarly to the A/D acquisition, the PWM imposes a low pass filter behavior.

It may be also worth to recall that the non-linear generation of side-band harmonics (e.g., side-band harmonics that are not alias of the small-signal input, but also depend on the $50\,\text{Hz}$ operation point) is not represented in (21) (a more elaborated modelling that considers low frequency side-band harmonics generation has been recently reported in [7]). For this specific study, neglecting non-linear components is assumed, which can be supported from different points of view: e.g., i) the existing normative states that high frequency non-linear effects should be disregarded when assessing the input-admittance passivity criterion (defined for linear systems) [16]; ii) the finite frequency approach also aims to avoid adding complexity in the very high frequency range [19], [20].

V. Experimental Verification

The procedure to measure $\mathbf{Y}(\omega)$ is inspired in the EN-50388 normative [5], [16], but extended to cover alias measurements.

This article has been accepted for publication in a future issue of this journal, but has not been fully edited. Content may change prior to final publication. Citation information: DOI 10.1109/TIE.2019.2892701, IEEE Transactions on Industrial Electronics

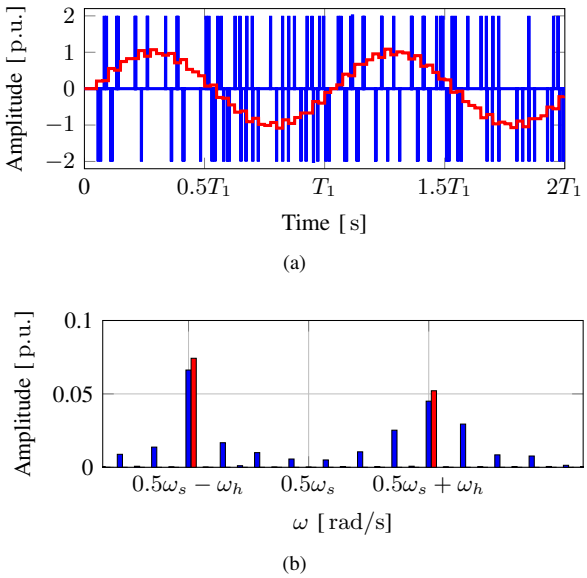

Fig. 6. High frequency components around the Nyquist frequency. (a) Time domain curves for a sampled signal which contains a high frequency small signal component over the fundamental (50 Hz) one (in red); in blue, its corresponding differential small-signal PWM signal [24]. (b) Spectrum of Fig. 6(a).

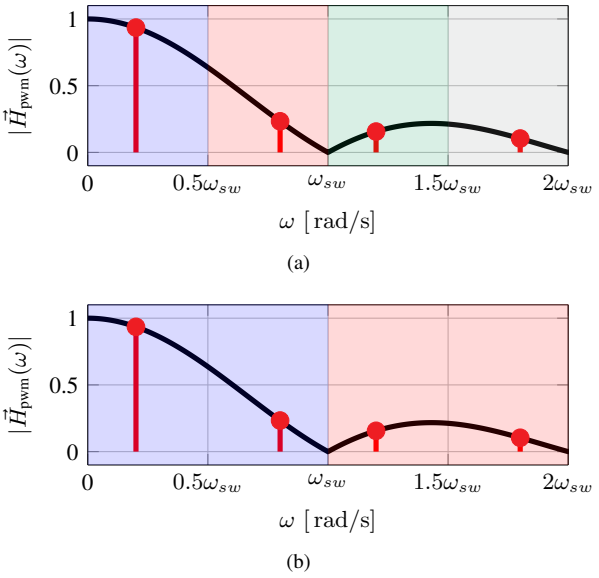

Fig. 7. Frequency response of PWM model. The back colors correspond to the alias regions defined in Fig. 5(a) (i.e., the controller rate defines the alias regions). (a) Single update implementation; it introduces a single component in each alias region. (b) Double update implementation; it introduces two components in each alias region.

From Fig. 1 inspection, the procedure is as follows: i) firstly, a voltage inter-harmonic over-imposed to the fundamental component is programmed at $e(t)$; ii) the converter control is activated with $i^{\text{ref}}(t) = 0$ and its steady state is reached quickly; iii) the time domain waveforms are stored for the different frequency points considered; iv) post-processing is made using a Matlab script; each $Y_{j,k}(\omega)$ component (with $j = 1, 2$ and $k = 1, 2$ for the experiments) is given by

$$Y_{j,k}(\omega) = \frac{|i_j(\omega)|^{\text{FFT}}}{|e_k(\omega)|^{\text{FFT}}}[\angle\phi^{\text{FFT}}_{i_j(\omega)} - \angle\phi^{\text{FFT}}_{e_k(\omega)}] \tag{24}$$

with the FFT superscript referring to data obtained by the Fast Fourier Transform (FFT).

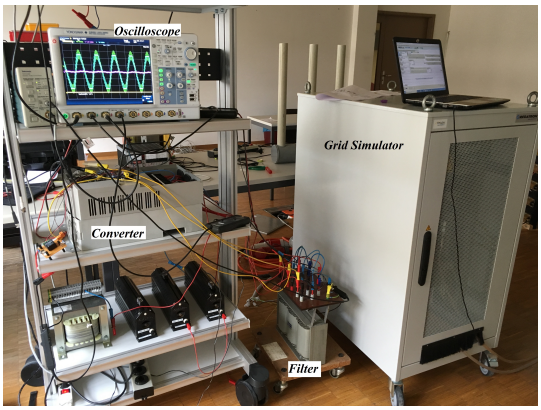

Fig. 8. Laboratory set-up.

Fig. 8 shows a photo of the lab-scale prototype, which is based on the system represented in Fig. 1. A LARA-100 development platform, which includes an industrial converter, its acquisition system and a *TMS320F28335* DSP, has been employed [27]. The grid waveform $e(t)$ is generated by a high performance grid simulator [28] with ability to introduce high-frequency high-amplitude perturbations; this device permits to over-impose arbitrary harmonics and inter-harmonics up to 3 kHz. In fact, in order to avoid the measurement to be polluted by uncontrolled sources of harmonic (e.g., PWM dead-time effects [29]) the measurements are obtained by injection of inter-harmonics (multiples of 25 Hz but not of 50 Hz). A reduced sampling rate is a requirement when frequency domain identification is sought for high frequencies using a grid simulator: e.g., $f_s = f_{sw} = 4$ kHz was employed in [5] to obtain measurements up to the Nyquist frequency. In order to show the aliasing effects, the sampling and switching frequencies have to be further reduced: $f_s = f_{sw} = 2$ kHz is employed in

TABLE I
EXPERIMENTAL PARAMETERS

Circuit	
Rated Power (transformer)	$S_{\text{max}} = 2\,\text{kW}$
Rated grid phase voltage	$E_{\text{rms}} = 100\,\text{V}$
Dc-link Voltage	$V_{dc} = 350\,\text{V}$
Dc-link Capacitor	$V_{dc} = 700\,\text{uF}$
Switching frequency	$\omega_{\text{sw}} = 2\pi 2000\,\text{rad/s}$
Grid frequency	$\omega_1 = 2\pi 50\,\text{rad/s}$
Converter inductance	$L = 20\,\text{mH}$
Converter equivalent resistance	$R = 1.2\,\Omega$
Controller	
Sampling frequency	$\omega_{\text{s}} = 2\pi 2000\,\text{rad/s}$
Proportional gain (dq-PI controller)	$k_{\text{p}} = 20\,\Omega$
Integral gain (dq-PI controller)	$k_{\text{i}} = 1200\,\Omega/\text{s}$
Active damping gain (dq-PI controller)	$k_{\text{ad}} = 100\,\mu\text{s}$
Proportional gain (dc-link controller)	$k_{\text{p}}^{\text{dc}} = 0.1 \quad [1/\Omega]$
Integral gain (dc-link controller)	$k_{\text{i}}^{\text{dc}} = 0.1 \quad [1/\Omega \cdot s]$

This article has been accepted for publication in a future issue of this journal, but has not been fully edited. Content may change prior to final publication. Citation information: DOI 10.1109/TIE.2019.2892701, IEEE Transactions on Industrial Electronics

this work. The selection of such a low controller sampling rate allows (the grid simulator) to inject high amplitude voltage alias (i.e., components above $f_s/2 = 1\,\mathrm{kHz}$) through the controller perturbation path [cf. $e(t)$ in Fig. 1] and hence obtain measurements for the identification of different $\mathbf{Y}(\omega)$ components. It is worth mentioning that the bandwidth of the anti-aliasing filters is higher than f_s, so it is assumed that they are not shaping $\mathbf{Y}(\omega)$. A Yokogawa DLM400 oscilloscope working at the high resolution of 12 bits has been employed to get the current and voltage measurements needed for the experimental $\mathbf{Y}(\omega)$ curve. The high resolution feature of the acquisition permits to limit the deviation standard below of $0.2\,\mathrm{deg}$ [30]. According to the EN50388 Ed. 2 standard, the real-time measurements have been obtained with the converter working as a rectifier at no-load conditions [16], but in practice a dc-link voltage controller compensating for the losses of the system has been activated. Table I shows the main parameters of the lab-scale experimental set-up. The controller gains have been obtained following guidelines of [5].

Fig. 9(a) shows a representative sample of time domain waveforms employed to get results of alias interactions. Fig. 9(b) includes the corresponding harmonic spectra. It can be appreciated how the line to line voltage is highly distorted by a high-frequency ($1775\,\mathrm{Hz}$) component over-imposed to the fundamental component ($50\,\mathrm{Hz}$). The amplitude of the perturbation signal ($60\,\mathrm{V}$ peak) is around 1/4 of the $50\,\mathrm{Hz}$ line-to-line voltage; this value allows to sense all the needed current measurements without much compromising the normal behavior of the converter. The resulting current has a dominant component of $50\,\mathrm{Hz}$, which compensates the losses and keeps the dc-link average value constant. Other high frequency components can be observed. They include side-band switching harmonics, non-linear low order harmonics and components that arise as a response to the perturbation. Clearly, a carefully study in the frequency domain requires to identify which components are due to the linear response of the system to an input perturbation and discard the ones due to a non-linear nature of the system (i.e., to discard the main source of measurement noise, which is associated to integer harmonics). As a practical countermeasure, it has been found that injection of components which are multiples of $25\,\mathrm{Hz}$ but not of $50\,\mathrm{Hz}$ permits a good discrimination of perturbation responses from non-linear components. Due to this fact, the current waveforms show a $25\,\mathrm{Hz}$ symmetry.

Fig. 10 shows the experimental results obtained with the system with active damping disabled and enabled. The results are compared to the theoretical model (depicted with $N = 4$). Since results are shown for the main part of the spectrum and the first alias range (i.e., $N = 2$ in the experiments), the theoretical models are obtained by cascading $Y_{11}(\omega_z)$ and $Y_{22}(\omega_z)$ in the frequency domain. So the system order for the experiments is $N = 2$: fundamental region and a first region of alias. It should be mentioned that, besides the limitations of the grid-simulator as a perturbation injection device, reliable measurements also tend to become unfeasible as the perturbation frequency increases (e.g., beyond $2\,\mathrm{kHz}$ in these experiments): in practice, the measured current components are more and more attenuated and, in then, difficult to distinguish from the measurement noise. From the results it can be checked that the active damping is very effective in the region around $f_s/4$ (i.e., slightly above the closed-loop controller bandwidth), where the control action compensates for delays effect that may create electric resonances [3], [5], [9]. This results is in accordance with the fact that effective active damping techniques are suitable for compensation delay effects in this region of the spectrum [3], [5], [9]. At higher frequencies, even beyond the Nyquist frequency, a phase-response in the vicinity of $-90\,\mathrm{deg}$ is predicted by the proposed models, which are well matching the experimental results. Still, due to the "aggressiveness" of active damping control, moderate excursion inside the forbidden region are

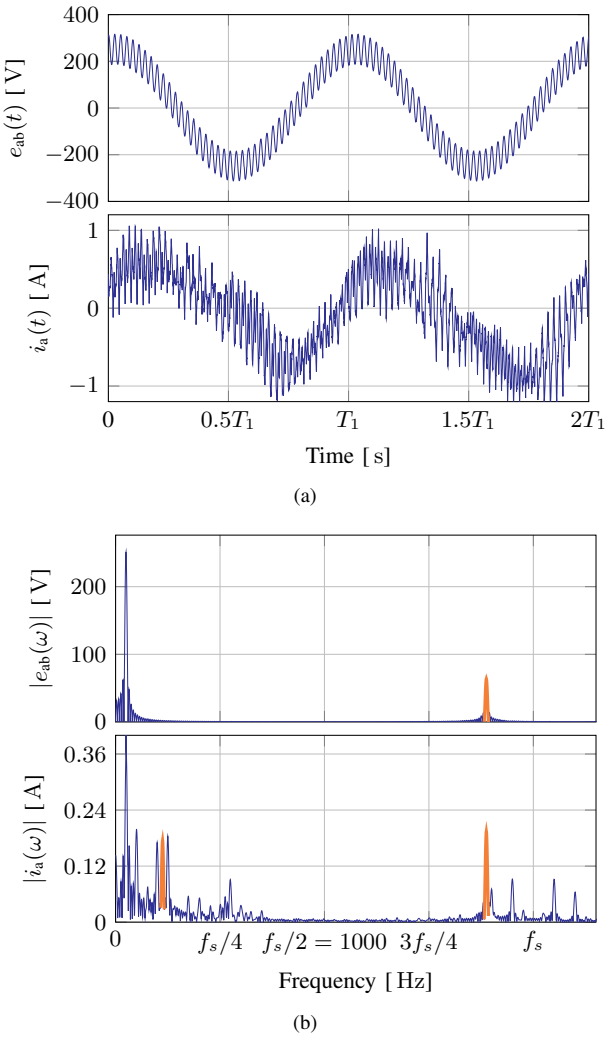

Fig. 9. An example of an experimental measurement for identification of two components of $\mathbf{Y}(\omega)$, including a perturbation signal with a frequency beyond the Nyquist frequency. a) Time-domain waveforms including a $1775\,\mathrm{Hz}$ perturbation of a $60\,\mathrm{V}$ peak amplitude, which is programmed in phase a and reflected in the line voltage; the resulting current is distorted with multiple components. b) Frequency domain measurements corresponding to Fig. 9(a) waveforms obtained by FFT. The linear perturbation source and its responses are highlighted in orange. Inter-harmonics perturbations have been found as an effective method to distinguish linear responses from the background non-linear distortion, mainly reflected as low order harmonics.

This article has been accepted for publication in a future issue of this journal, but has not been fully edited. Content may change prior to final publication. Citation information: DOI 10.1109/TIE.2019.2892701, IEEE Transactions on Industrial Electronics

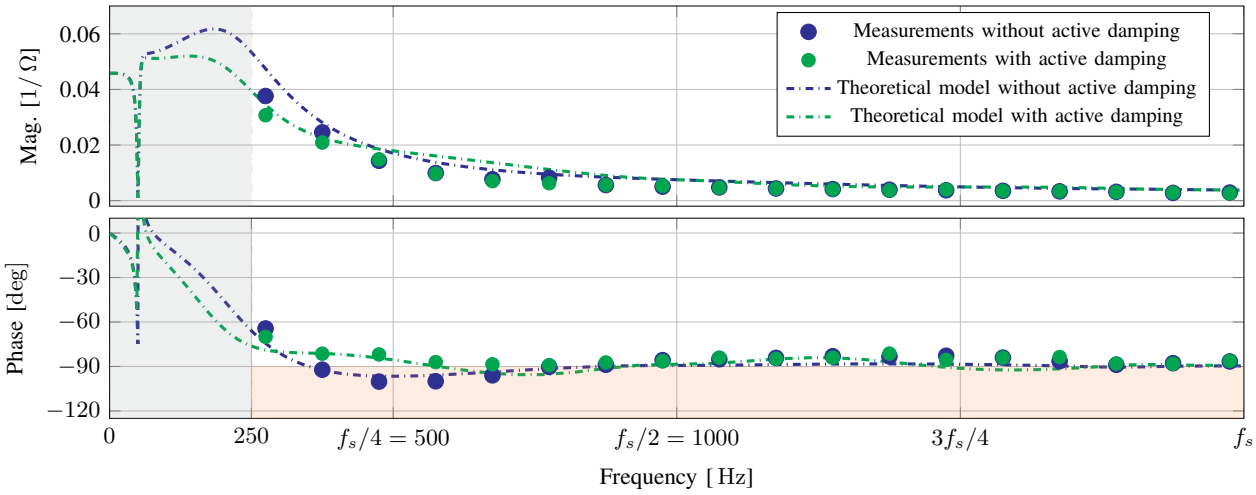

Fig. 10. Input-admittance measurements with/without active damping action. The gray region corresponds to the low frequency region, where passivity compliance is not checked in the EN50388. The orange region is forbidden for passivity compliance.

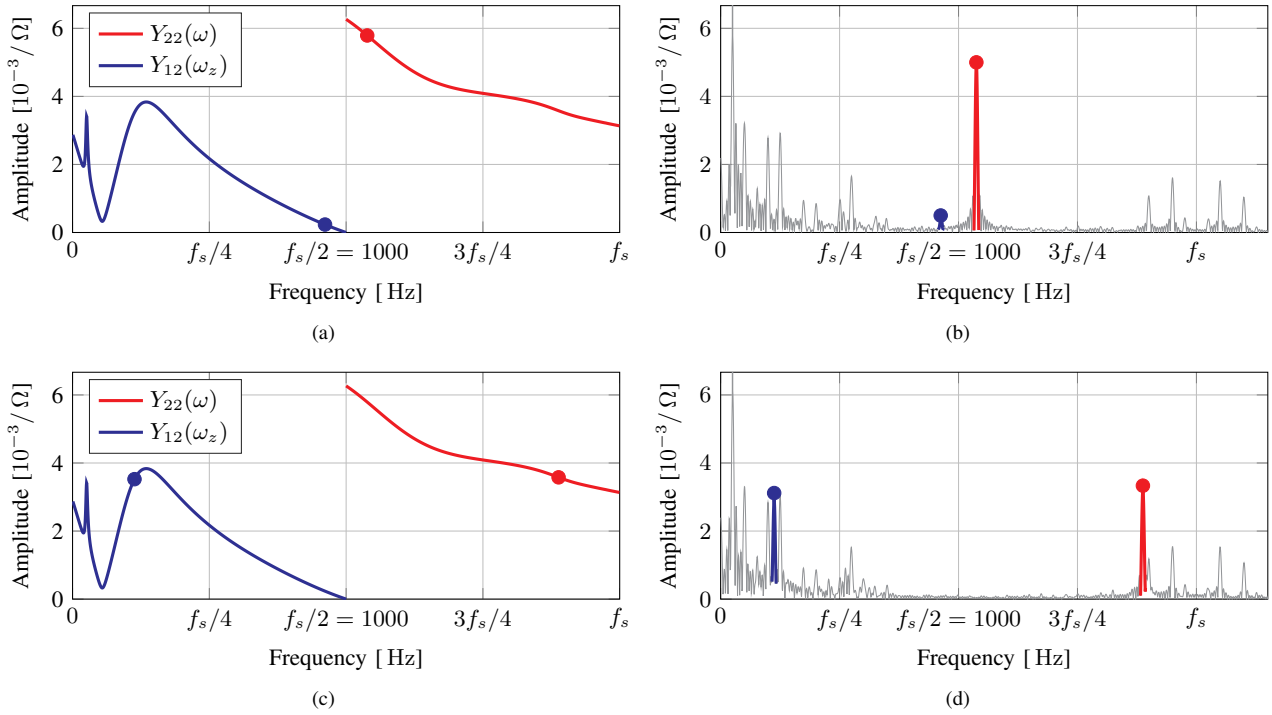

Fig. 11. Current spectrum for perturbations above $\omega_s/2$; perturbation at $1075\,\mathrm{Hz}$ and $1775\,\mathrm{Hz}$. (a) Theoretical points over the corresponding theoretical admittances for the perturbation at $1075\,\mathrm{Hz}$. (b) Amplitude measurements (with FFT) for the perturbation at $1075\,\mathrm{Hz}$. (c) Theoretical points over the corresponding theoretical admittances for the perturbation at $1775\,\mathrm{Hz}$. (d) Amplitude measurements (with FFT) for the perturbation at $1775\,\mathrm{Hz}$.

predicted when this is enabled, which is in accordance with [8]. Furthermore, the proposed model also reflects the gradual loss of control action as the frequency increases, which is also in good agreement with [5], [21]. In other words, despite passivity properties may be slightly compromised in the high frequency region, active damping to compensate for delay in the relative low frequency range seems a suitable technique overall. This former assessment is in good agreement with the finite frequency design principles of [19], [20].

Fig. 11 shows experimental results obtained when the frequency injection considers aliasing terms. The idea of this measurements is to show how aliasing is reflected inside the controller actuation. For these measurements, active damping is enabled, since the derivative action tends to amplify the high frequency component. Overall, these key results show that, when the perturbation is near $0.5\omega_s$, the fundamental component is small, since the acquisition filtering tends to cancel out these components. However, aliasing components

This article has been accepted for publication in a future issue of this journal, but has not been fully edited. Content may change prior to final publication. Citation information: DOI 10.1109/TIE.2019.2892701, IEEE Transactions on Industrial Electronics

near ω_s may be amplified, since they are seen as low frequency components in the discrete systems. It can be checked again that Fig. 11 shows a good agreement between theoretical expectations and measurements.

Once the accuracy of the model is proved, Fig. 12 is included to extend the theoretical assessment. Fig. 12 shows theoretical curves that compare the aliasing terms (the active damping is enabled). It can be checked that, despite the derivative term amplifies the alias terms, the amplitudes of non-diagonal terms of $\mathbf{Y}(\omega_z)$ are much smaller than $|Y_{11}(\omega_z)|$ [it should be noticed that $|Y_{11}(\omega_z)|$ is scaled down in Fig. 12]. From the point of view of multi-variable control this has some important implications: $\mathbf{Y}(\omega_z)$ can be assumed as a diagonal matrix, and hence the dynamic interactions with the grid will only depend on the diagonal component [31]. In other words, for any frequency ω, the passivity compliance defined by its corresponding diagonal terms [14], [19]. Fig. 12(b) assess the influence of the $\mathbf{Y}(\omega_z)$ order in the accuracy of the model. The simplest model, which corresponds to $N = 1$ (i.e., it discards the aliases components), gives an inaccurate and pessimistic estimation around the Nyquist frequency [cf. phase curve at the $(f_s/4, f_s/2)$ region]. An accurate modeling is achieved when alias components are considered; i.e., models with $N = 2$ and $N = 4$. It is also noticed that the weight of higher aliases in the low frequency region of the spectrum drastically decreases: a theoretical model with $N = 2$ is accurate enough to support the experimental results, which is also in a good accordance with the finite frequency principles of [19], [20].

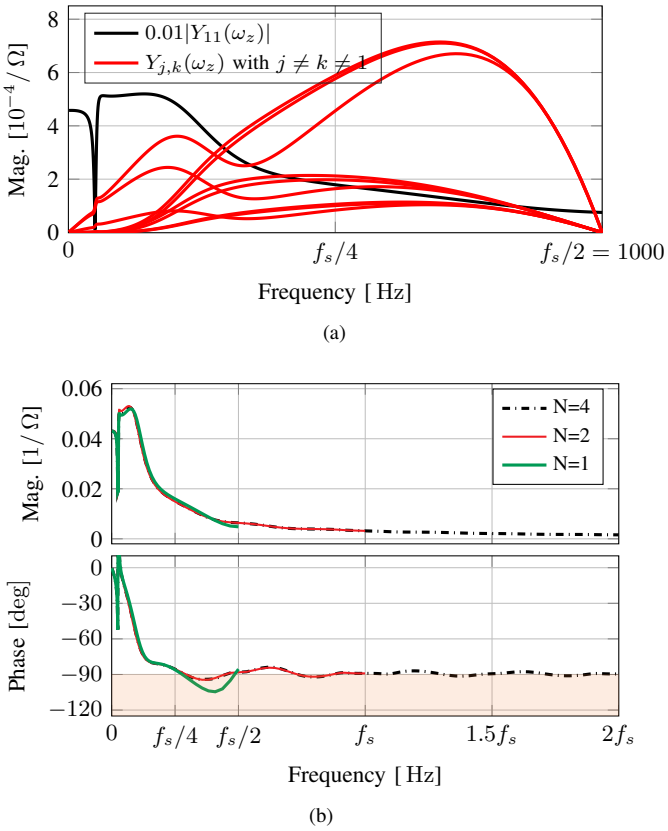

Fig. 12. Influence of N in the model. (a) Magnitudes of $\mathbf{Y}(\omega_z)$ alias terms [the red curves are $Y_{j,k}(\omega_z)$ with $j \neq k \neq 1$ up to $N = 4$] versus $0.01|Y_{11}(\omega_z)|$ (black curve, notice the 0.01 factor). (b) Input-admittance [i.e., diagonal terms of $\mathbf{Y}(\omega_z)$] for different N values.

VI. Conclusions

A multi-variable input-admittance model for grid-connected converters, namely $\mathbf{Y}(\omega_z)$, has been developed and experimentally verified. The work is motivated by recent works in which design for passivity methods tends to present whack-a-mole scenarios, in which compensation at a relatively low-frequency region of the spectrum (e.g., by active damping techniques) implies to worsen the dynamics at higher frequencies. Therefore, a main objective of the work is to accurately represent and assess the likelihood and severity of harmonic instability issues in all regions of the spectrum. To do so, $\mathbf{Y}(\omega_z)$ should accurately reflect system delays, but also low-pass filter behaviors that tend to reduce the feedback control actuation. A step-by-step detailed modelling, specially focused on the discrete-operation (i.e., A/D acquisition, discrete controllers and PWM blocks) is provided. Comprehensive experimental validations aimed to obtain results in the high frequency regions of the spectrum have been performed. The figures of merit show the accuracy of the model, which includes main components and also responses to input alias perturbations. From the point of view of dynamics implications, it is observed most critical zone of the spectrum is the region slightly above the theoretical control bandwidth, where the controller action is still non-negligible; however, at very high frequencies, the excursions into the non-passivity zone are very smooth, and, in practice, the input-admittance behaves as an inductive filter; i.e., irrespectively from controller actions, at high frequencies, the imaginary part of the input-admittance diagonal terms weights much more than its corresponding real part. Therefore, in accordance with finite frequency design rules, active damping to compensate for delay in the relative low frequency range seems a suitable technique overall, despite passivity properties may be slightly compromised in the high frequency region.

Appendix

This appendix shows basic theory and an example of application of SISO impedance modelling and application for dynamics assessment of grid-connected converter [3], [9], [12]. Fig. 13(a) depicts the key modelling idea: the grid model and the converter are represented by Thevenin/Norton linear equivalents; i.e., there is a representation in the frequency domain for $Z_g(\omega)$ and $Y(\omega)$. System modelling can be obtained by analytic methods [3], [9] or from perturbation and system identification [12]. After modelling, the dynamics of the whole system is a function of the minor loop gain product, which is defined as $Z_g(\omega)Y(\omega)$. Basic SISO control techniques, such as Bode, root-locus and Nyquist criteria are suitable to find the dominant responses of the system [3], [9], [12], [15]. In fact, the minor loop implicity defines the responses of the sensitivity function [9], [15]

$$S(\omega) = \frac{1}{1 + Z_g(\omega)Y(\omega)}. \tag{25}$$

This article has been accepted for publication in a future issue of this journal, but has not been fully edited. Content may change prior to final publication. Citation information: DOI 10.1109/TIE.2019.2892701, IEEE Transactions on Industrial Electronics

By definition, the poles of $S(\omega)$ are reflected in all the responses of the system [9], [15], [31]. By using Nyquist diagrams for the assessment, the inverse sensitivity peak η is a reliable stability margin: the higher η the more damped system [9], [31]; $\eta < 0.5$ is a reasonable criterion to define poorly damped systems [31].

As an insightful example, Fig. 13(b) shows the Nyquist trajectories of two different stable systems. Assuming the absence of right half poles in $Z_g(\omega)$ and $Y(\omega)$, an unstable system would be reflected in a trajectory encircling the critical point -1. Case 1 shows a scenario in which the system is poorly damped; case 2 shows a system with more relative stability. Subsequently, Fig. 13(c) shows the impulse responses for each sensitivity function. The poorly damped system shows a less attenuated oscillation in the time domain (an unstable system would be reflected in exponentially increasing oscillations).

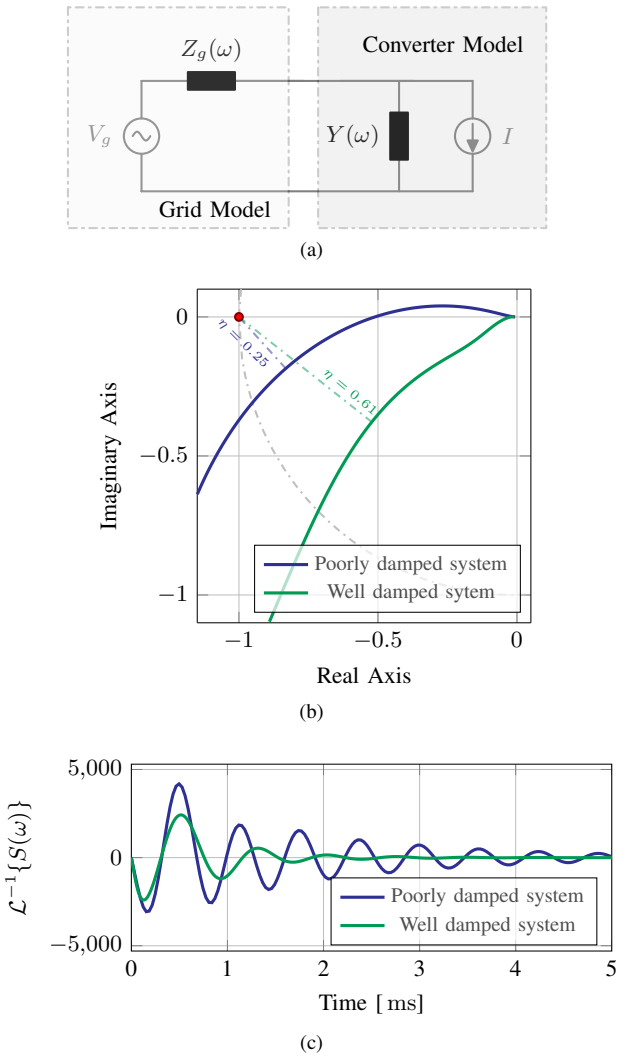

Fig. 13. Impedance stability criterion for grid-connected power converter. (a) Basic formulation: the stability of the system depends on grid impedance and converter input-admittance definitions in the frequency domain [3], [9], [12], [15]. (b) Nyquist diagram for two different scenarios. (c) Impulse response of the corresponding sensitivities from Fig. 13(b).

REFERENCES

[1] E. Mollerstedt and B. Bernhardsson, "Out of control because of harmonics-an analysis of the harmonic response of an inverter locomotive," *IEEE Control Syst. Mag.*, vol. 20, no. 4, pp. 70–81, 2000.

[2] X. Wang and F. Blaabjerg, "Harmonic stability in power electronic based power systems: Concept, modeling, and analysis," *IEEE Trans. Smart Grid*, vol. to be published, 2018.

[3] L. Harnefors, A. G. Yepes, A. Vidal, and J. Doval-Gandoy, "Passivity-based controller design of grid-connected vscs for prevention of electrical resonance instability," *IEEE Trans. Ind. Electron.*, vol. 62, no. 2, pp. 702–710, 2015.

[4] A. Rygg, M. Molinas, C. Zhang, and X. Cai, "On the equivalence and impact on stability of impedance modeling of power electronic converters in different domains," *IEEE J Emerg Sel Top Power Electron*, vol. 5, no. 4, pp. 1444–1454, Dec. 2017.

[5] E. Rodriguez-Diaz, F. D. Freijedo, J. M. Guerrero, J.-A. Marrero-Sosa, and D. Dujic, "Input-admittance passivity compliance for grid-connected converters with LCL filter," *IEEE Trans. Ind. Electron.*, vol. to be published, 2018.

[6] R. Luhtala, T. Roinila, and T. Messo, "Implementation of real-time impedance-based stability assessment of grid-connected systems using MIMO-identification techniques," *IEEE Trans. Ind. Appl.*, vol. to be published, 2018.

[7] D. Yang, X. Wang, and F. Blaabjerg, "Sideband Harmonic Instability of Paralleled Inverters With Asynchronous Carriers," *IEEE Trans. Power Electron.*, vol. 33, no. 6, pp. 4571–4577, Jun. 2018.

[8] L. Harnefors, R. Finger, X. Wang, H. Bai, and F. Blaabjerg, "Vsc input-admittance modeling and analysis above the Nyquist frequency for passivity-based stability assessment," *IEEE Trans. Ind. Electron.*, vol. 64, no. 8, pp. 6362–6370, Aug. 2017.

[9] F. D. Freijedo, E. Rodriguez-Diaz, M. S. Golsorkhi, J. C. Vasquez, and J. M. Guerrero, "A Root-Locus Design Methodology Derived from the Impedance/Admittance Stability Formulation and Its Application for LCL Grid-Connected Converters in Wind Turbines," *IEEE Trans. Power Electron.*, vol. 32, no. 10, pp. 8218 – 8228, Oct. 2017.

[10] M. Cespedes and J. Sun, "Impedance modeling and analysis of grid-connected voltage-source converters," *IEEE Trans. Power Electron.*, vol. 29, no. 3, pp. 1254–1261, 2014.

[11] L. H. Kocewiak, J. Hjerrild, and C. L. Bak, "Wind turbine converter control interaction with complex wind farm systems," *IET Renewable Power Generation*, vol. 7, no. 4, pp. 380–389, 2013.

[12] J. Sun, "Impedance-based stability criterion for grid-connected inverters," *IEEE Trans. Power Electron.*, vol. 26, no. 11, pp. 3075–3078, 2011.

[13] J. L. Agorreta, M. Borrega, J. Lopez, and L. Marroyo, "Modeling and control of n-paralleled grid-connected inverters with lcl filter coupled due to grid impedance in PV plants," *IEEE Trans. Power Electron.*, vol. 26, no. 3, pp. 770–785, Mar. 2011.

[14] L. Harnefors, M. Bongiorno, and S. Lundberg, "Input-admittance calculation and shaping for controlled voltage-source converters," *IEEE Trans. Ind. Electron.*, vol. 54, no. 6, pp. 3323–3334, 2007.

[15] J. Liu, X. Feng, F. C. Lee, and D. Borojevich, "Stability margin monitoring for dc distributed power systems via perturbation approaches," *IEEE Trans. Power Electron.*, vol. 18, no. 6, p. 12541261, Nov 2003.

[16] *EN50388 Ed.2. Railway Applications – Power supply and rolling stock – Technical criteria for the coordination between power supply (substation) and rolling stock to achieve interoperability*, Cenelec Std., 2012.

[17] D. Dujic, C. Zhao, A. Mester, J. K. Steinke, M. Weiss, S. Lewdeni-Schmid, T. Chaudhuri, and P. Stefanutti, "Power electronic traction transformer-low voltage prototype," *IEEE Trans. Power Electron.*, vol. 28, no. 12, pp. 5522–5534, 2013.

[18] F. D. Freijedo, D. Dujic, and J. A. Marrero-Sosa, "Design for passivity in the z-domain for LCL grid-connected converters," in *Proc. of the IEEE Industrial Electronics Society Annual Conference*, Firenze, Italy, Oct. 2016, pp. 7016–7021.

[19] T. Iwasaki, S. Hara, and H. Yamauchi, "Dynamical system design from a control perspective: Finite frequency positive-realness approach," *IEEE Trans. Autom. Control*, vol. 48, no. 8, pp. 1337–1354, 2003.

[20] J. R. Forbes and C. J. Damaren, "Synthesis of Optimal Finite-Frequency Controllers Able to Accommodate Passivity Violations," *IEEE Trans. Control Syst. Technol.*, vol. 21, no. 5, pp. 1808–1819, Sep. 2013.

[21] C. M. Wolf, M. W. Degner, and F. Briz, "Analysis of current sampling errors in pwm vsi drives," *IEEE Trans. Ind. Appl.*, vol. 51, no. 2, pp. 1551–1560, 2015.

[22] B. Kuo, "A Z-transform-describing-function for on-off type sampled-data systems," *Proc. of the IRE*, vol. 48, no. 5, pp. 941–942, 1960.
[23] A. Gelb and W. E. V. Velde., *Multiple-Input Describing Functions and Nonlinear System Design.*, M. Hill, Ed., 1968.
[24] H. du Toit Mouton, S. M. Cox, B. McGrath, L. Risbo, and B. Putzeys, "Small-signal analysis of naturally-sampled single-edge pwm control loops," *IEEE Trans. Power Electron.*, vol. 33, no. 1, pp. 51–64, 2018.
[25] C. L. Phillips and H. T. Nagle, *Digital Control System Analysis and Design (Third Edition)*, I. Prentice-Hall, Ed., 1995.
[26] H. d. T. Mouton, B. McGrath, D. G. Holmes, and R. H. Wilkinson, "One-dimensional spectral analysis of complex PWM waveforms using superposition," *IEEE Trans. Power Electron.*, vol. 29, no. 12, pp. 6762–6778, Dec. 2014.
[27] Perun Technologies, *LARA-100 Motherborad User Manual*, 2016. Available: www.perun-power.com [Accessed: July 21, 2018].
[28] Regatron AG, "Topcon tc.acs full 4-quadrant grid simulator," 2014.
[29] D. G. Holmes and T. A. Lipo, *Pulse Width Modulation for Power Converters: Principles and Practice*, IEEE Press, 2003.
[30] N. Locci, C. Muscas, L. Peretto, and R. Sasdelli, "A numerical approach to the evaluation of uncertainty in nonconventional measurements on power systems," *IEEE Trans. Instrum. Meas.*, vol. 51, no. 4, pp. 734–739, Aug. 2002.
[31] G. C. Goodwin, S. F. Graebe, and M. E. Salgado, *Control System Design*. Prentice Hall, 2000.

Francisco D. Freijedo (M'07-SM'16) received the M.Sc. degree in physics from the University of Santiago de Compostela, Santiago de Compostela, Spain, in 2002 and the Ph.D. degree in Electrical Engineering from the University of Vigo, Vigo, Spain, in 2009. From 2005 to 2011, he was a Lecturer in the Department of Electronics Technology, University of Vigo. From 2011 to 2014, he worked in Gamesa Innovation and Technology as a Power Electronics Control Engineer, where he was involved in Wind Energy projects. From 2014 to 2016, he was a Postdoctoral Researcher in the Department of Energy Technology, Aalborg University. Since 2016, he is a Scientific Collaborator of the Power Electronics Laboratory, Ecole Polytechnique Federale de Lausanne. His research interests include many power conversion technologies and challenging control problems.

Marc Ferrer received his B.Sc and M.Sc degrees in Industrial Engineering from the Escola Tecnica Superior d'Enginyeria Industrial de Barcelona, Universitat Politecnica de Catalunya, Catalunya, Spain, in 2015 and 2018, respectively. He did his M.Sc final project at the Power Electronics Laboratory of the Ecole Polytechnique Federale de Lausanne, Lausanne, Switzerland. Since May 2018, he is a Software Control Application Engineer at Lear Corporation. He is interested in Power Electronics modeling, design and control, with special focus on E-mobility applications.

Drazen Dujic (S'03-M'09-SM'12) received the Dipl.-Ing. and M.Sc. degrees from the University of Novi Sad, Novi Sad, Serbia, in 2002 and 2005, respectively, and the Ph.D. degree from Liverpool John Moores University, Liverpool, U.K., in 2008, all in Electrical Engineering. From 2002 to 2006, he was a Research Assistant with the Department of Electrical Engineering, University of Novi Sad. From 2006 to 2009, he was a Research Associate with Liverpool John Moores University. From 2009 to 2013, he was with the ABB Corporate Research Center, Switzerland, as a Principal Scientist working on Power Electronics Projects. During 2010-2011, he was involved in the development of the Power Electronic Traction Transformer (PETT). From 2013 to 2014, he was with ABB Medium Voltage Drives, Turgi, Switzerland, as an R&D Platform Manager. He is currently an Assistant Professor with the Ecole Polytechnique Federale de Lausanne, Lausanne, Switzerland, where he is also the Director of the Power Electronics Laboratory. He has authored/coauthored more than 100 scientific publications and has filed 11 patents. His current research interests include the areas of design and control of advanced high-power electronics systems and high-performance drives. Dr. Dujic is an Associate Editor for the IEEE TRANSACTIONS ON INDUSTRIAL ELECTRONICS, IEEE TRANSACTIONS ON POWER ELECTRONICS, and IET Electric Power Applications. He received the First Prize Paper Award form the Electrical Machines Committee of the IEEE IES at the IECON 2007. In 2014, he received the Isao Takahashi Power Electronics Award for outstanding achievement in power electronics.